Effect of Aspect Ratio on the Catalytic Activities of Gold Nanorods

Lubna Khalil[1] · Sana Sabahat[1] · Waqqar Ahmed[2]

Abstract

Gold nanoparticles have shown great potential for heterogeneous catalysis. Herein, we show that the catalytic efficiency of gold nanorods (Au NRs) depends sensitively on their aspect ratio. The high-energy side facets of Au NRs play a crucial role in their catalytic efficiency. We have synthesized Au NRs of three different aspect ratios using a modified seed-mediated method. The aspect ratio of Au NRs increased from 2.3 to 4.6 and then to 5.4 with the addition of different concentrations of HNO_3 in the growth solution. The synthesized Au NRs with different aspect ratios were tested for their catalytic activity towards the reduction of various organic pollutants such as 4-nitrophenol (4-NP), methylene blue (MB), and methyl orange (MO). It was found that for the same gold content, nanorods with a larger surface area of the high-energy side facets, irrespective of the overall surface area, were more effective catalysts in all cases.

Graphical Abstract
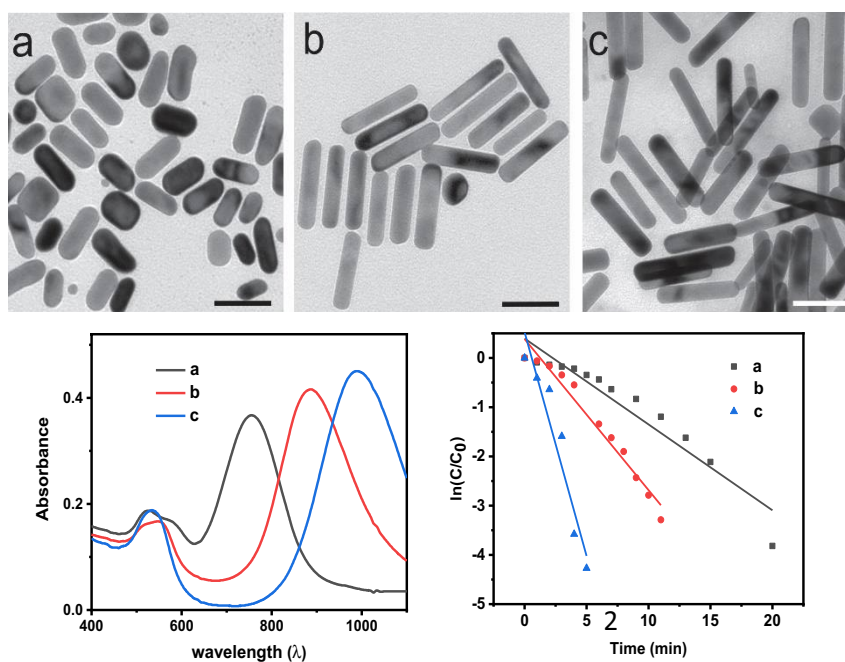
Extended author information available on the last page of the article

1 Introduction

During the last few decades, Au nanoparticles have attracted great attention due to their size- and shape-dependent characteristics that make them interesting for a variety of applications [1–5]. One of the important applications of gold nanoparticles is their use as a catalyst for various reactions. In the 1970s Bond et al. showed the unexpected catalytic activity of Au on boehmite for the hydrogenation of alkyne in the presence of alkenes [6]. This was followed by the impressive work of Haruta et al. on the low-temperature oxidation of CO [7], and Hutchings on the hydrochlorination of ethyne using Au as a catalyst of choice in the 1980s [8]. More recently, Au nanoparticles have begun to be employed in various industries, especially the chemical and pharmaceutical industries [9].

The catalytic performance of Au nanoparticles depends sensitively on their size and shape [10]. The surface area and surface energy play a crucial role in the comparative catalytic performance of the various Au nanoparticle morphologies. Therefore, there is great interest in optimizing the synthesis of Au nanoparticles for their best catalytic performance. The anisotropic nanoparticles e.g. NRs are especially interesting owing to their higher surface area and the presence of a high concentration of low coordination atoms which act as catalytic hotspots. Various comparative studies for morphology-dependent catalysis have been conducted, but often with conflicting results. Kundu et al. showed that gold nanospheres were catalytically most active than Au NRs and nanoplates for the model reaction of catalytic reduction of 4-NP to 4-AP [11]. On the other hand, Jiji et al. showed that Au NRs were catalytically more active than gold nanospheres [12]. However, in addition to the morphology, the types of facets covering the surface for a certain particle shape can also have a marked influence on the catalytic activity. For example, Zhang et al. showed that the presence of high-indexed facets on gold nanoparticles enhanced their catalytic performance due to the presence of a higher fraction of surface atoms with low coordination [13].

Gold NRs are known to consist of higher energy side facets and lower energy end facets [14]. Therefore, the relative surface area of the side and end facets, which changes with the change in their aspect ratio, can affect their catalytic efficiency. Herein, we show that an increase in the aspect ratio of Au NRs can significantly increase their catalytic activity. We demonstrate the catalytic conversion of 4-NP to 4-AP and the catalytic degradation of MB and MO. Gold NPs of different aspect ratios were synthesized with the seed-mediated method. The aspect ratio was simply controlled by tuning the pH of the reaction medium. The NRs having a higher aspect ratio were found to be more effective for the catalytic reduction of 4-NP, MB and MO.

2 Materials and Methods

2.1 Materials

Chemicals used for the synthesis are cetyltrimethylammonium bromide (CTAB), chloroauric acid, sodium borohydride (NaBH$_4$), ascorbic acid, nitric acid (HNO$_3$) and silver nitrate (AgNO$_3$). For washing purposes deionized (DI) water, and aqua regia were used.

2.2 Synthesis of Au NRs by Seed Mediated Method

For the synthesis of Au NRs, we used a seed-mediated method. It is a two-step process.

2.2.1 Preparation of Gold Seeds

100 µl of 0.025 M HAuCl$_4$ solution was added into (10 ml, 0.1 M) CTAB solution. Then, 450 µl of 0.02 M freshly prepared NaBH$_4$ was added under vigorous stirring. After the addition of NaBH$_4$, the color of the solution turned brown, indicating particle formation. The seed solution was aged at 35 °C for 2–3 h before use.

2.2.2 Preparation of Growth Solution

Three Au NRs samples were prepared. For each one, 100 µl of 0.025 M HAuCl$_4$ solution was added into (5 ml, 0.1 M) CTAB solution contained in a clean scintillation vial. Subsequently, 5 µl of 0.1 M AgNO$_3$ was added. Next, 1 ml and 1.5 ml of 0.1 M HNO$_3$ was added to two different vials, and the samples were labeled as R2 and R3, respectively. No acid was added to the third sample (labeled as R1). Subsequently, 35 µl of freshly prepared ascorbic acid (0.1 M) was added to each sample. For R1, the sample became colorless instantly while for R2 and R3 they became colorless within a few mins due to the slower reaction kinetics owing to the relatively lower pH of these growth solutions. Finally, 10 µl of seed solution was added to each vial. The resultant mixture was kept undisturbed at 30 °C for overnight to grow. The appearance of reddish color in the growth solution indicated the growth of the seeds. In this case, as well, the color appeared later for the samples with lower pH of the growth solution due to the presence of acid.

2.3 Characterization

The AuNR formation was initially confirmed with UV–Vis spectroscopy. To investigate the size and shape of AuNRs, transmission electron microscopy (TEM) was carried out. The catalytic activity of synthesized AuNRs was monitored by a UV–Vis spectrophotometer.

2.4 Catalysis

To assess the effect of different AR on the catalytic properties of Au NRs, we investigate the catalytic reduction of 4-nitrophenol (4-NP), methylene blue (MB) and methyl orange (MO). For this purpose, we carried out an experiment in which 1 ml of 0.1 M $NaBH_4$ solution was added to 3 ml of either 5×10^{-5} M 4-NP, MO or MB. As discussed in the subsequent section, the yield i.e. conversion of Au ions to Au(0) is different for three Au NRs samples, therefore, we added different volumes of each AuNR sample in the reaction medium to keep the concentration of added Au atoms the same in all cases. For 4-NP and MO, 19 µl, 21 µl and 23 µl of R1, R2 and R3 solutions, respectively, were added. For MB, 37 µl, 42 µl and 46 µl of R1, R2 and R3, respectively, have been added. The Au NRs solution in 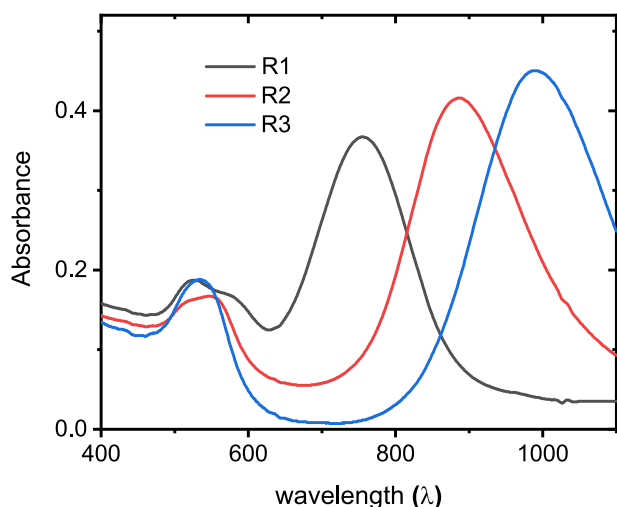all cases was added under vigorous stirring to make sure the efficient mixing of the catalysts. However, after a few seconds, the stirring was stopped. The reaction was observed with a UV–Vis spectrometer.

3 Results and Discussions

Figure 1 shows the UV–Vis absorption spectra of the synthesized Au NRs. For all samples, the characteristic transverse and longitudinal plasmon peaks are present. Moreover, there is a clear red shift in the longitudinal plasmon peak position with an increase in the concertation of HNO_3 in the growth solution. The red shift in the longitudinal plasmon peak indicates the increase in the aspect ratio of NRs [15].

Another consequence of the lower reducing power of ascorbic acid is the reduction in the Au ions to Au(0) conversion yield. As discussed before, the seed-mediated method of Au NRs does not provide 100% conversion of Au ions to Au(0). The concentration of Au(0) atoms in the product can be found by measuring the absorbance value at 400 nm [16]. It is well established that the absorbance value at 400 nm is entirely due to the interbond transitions. An absorbance value of 1 corresponds to the molarity of 0.4 mM of Au(0) [16]. The estimated concentration of Au(0) in our case is 0.0628 mM, 0.0552 mM and 0.0508 mM for R1, R2 and R3. A slightly lower molar concentration for R2 and R3 is due to the added acid, which increases the overall volume of the Au NRs suspension. The Au ion to Au NRs conversion yield of about 13% for all samples.

Figure 2a–c depicts the TEM images of samples R1, R2 and R3, respectively. It can be easily seen that most of the synthesized Au NRs have a uniform rod-shaped morphology. The yield of nanorods is greater than 90% for all three samples. The average lengths of Au NRs are about 38 ± 6, 68 ± 12 and 71 ± 13 nm and the width are determined to be 16 ± 2, 15 ± 1.5 and 13 ± 1.9 nm. There is a clear increase

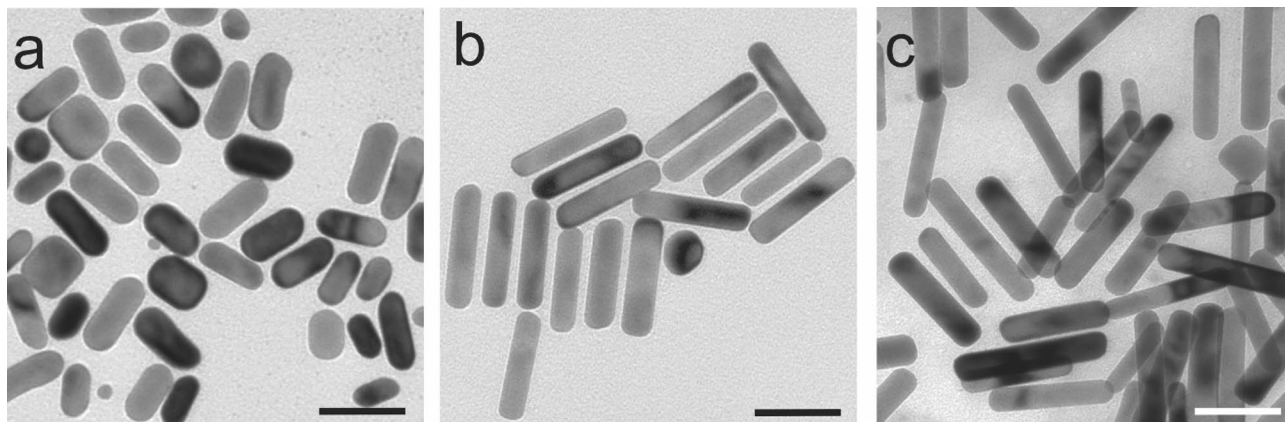**Fig. 1** UV–Vis spectra of Au NRs

Fig. 2 TEM images of samples R1 (**a**), R2 (**b**) and R3 (**c**); the scale bar is 50 nm in all cases

in length and decrease in the width of NRs with increasing HNO_3 concentration in the growth solution. Consequently, the aspect ratio of Au NRs also increases with the increase in HNO_3 concentration. The average aspect ratios for Au NRs are approximately 2.3, 4.6 and 5.4 for samples R1, R2 and R3, respectively. Therefore, the TEM results are consistent with the UV–Vis spectra.

The mechanism of the formation of Au NRs is debated in the literature. However, it is widely believed that with the addition of $HAuCl_4$ solution in the CTAB, chloride ions in the $AuCl_4^-$ are replaced with bromide ions. The resultant $AuBr_4^-$ makes a complex with cations of the surfactant i.e. CTA^+ [16]. This results in the cathodic shifting of the redox potential of Au ions. Under these reaction conditions, ascorbic acid can only partially reduce Au(III) ions to Au(I) [17–19]. With the addition of seeds, Au(I) ions reduce to Au(0) on top of the seeds due to the catalytic effect provided by the seeds. The synthesized seeds by our method are single-crystal CTAB capped with a size of 2–4 nm, as described in the previous reports [16]. These seeds grow by atom-by-atom deposition of Au monomers preferably on the end facets. There are different opinions about the type of side and end facets with which Au nanorods are bounded. But it seemed to be accepted now that the side facets are {520}, which have relatively higher energy compared to the end {111} and {100} facets [14]. Therefore, the side facets are more prone to the preferential adsorption of the surfactant, or the underpotential deposition of Ag, which directs the deposition of Au monomers to the end facets resulting in anisotropic growth. With the decrease in the pH of the reaction medium, the reducing power of the ascorbic acid decreases [20, 21]. Consequently, slower growth kinetics favors the preferred deposition of Au monomers onto the end facets, rather than the side facet, leading to the formation of Au NRs with higher aspect ratios.

3.1 Catalysis Reduction Reactions Using Au NRs

The catalytic reduction of 4-NP, MB and MO was carried out using Au NRs as catalysts. 4-NP is a phenolic compound also known as 4-hydroxynitrobenzene or p-Nitrophenol [22]. In general, it is used in the production of drugs (e.g. Acetaminophen), ethyl and methyl parathion, pesticide, antifungal agent, and dyes. 4-NP is an intermediate in the manufacturing of paracetamol [23]. In an aqueous environment, 4-NP shows a peak at 400 nm which decreases rapidly in the presence of $NaBH_4$ and Au NRs catalyst with time. Reduction of 4-NP results in the formation of 4-aminophenol (4-AP). The product peak for 4-AP appears gradually at 300 nm [24]. Figure 3a–c depicts the UV–Vis spectra of the reduction reaction. The peak at 400 nm decreases with time; there is an initial slower decrease which accelerates within a few mins. This could be due to the removal of the CTAB from

the Au NRs. Initially, Au NRs are covered by the bilayer of the CTAB. It has been reported that in the presence of a high concentration of $NaBH_4$ in the solution, which is relevant in this case, BH_4^- ions can replace the CTAB coting from the Au NRs [25]. Therefore, at the start, the reduction of 4-NP is slower but with the passage of time and the CTAB bilayer is removed from the Au NRs, more active surfaces are available for the reduction reaction to occur. Therefore, there is an increase in the catalytic degradation rate.

To find out the relative performance of catalysts, we carried out the linear fitting of the ln (C/C_0) versus the time plot (Fig. 3d). Here C is the instantaneous intensity and C_0 is the initial intensity of 4-NP. The apparent rate constants for R1–R3 were estimated as 0.17447, 0.307 and 0.909 min^{-1}, respectively. This indicates that with an increase in the aspect ratio of Au NRs, their catalytic capability increases. There is a five-fold increase in the apparent rate constant with the increase in aspect ratio from 2.3 to 5.4.

Methylene Blue (MB) is a cationic, thiazine dye that is one of the most frequently used substances in the dye industry [26, 27]. In an aqueous environment, MB shows maximum absorbance at 664 nm. In oxidized form it has an intense deep blue color; the reduced form leukomethylene blue (LMB) is a colorless product [28, 29]. The catalytic degradation of MB into LMB was investigated in the presence of $NaBH_4$, and by employing Au NRs as a catalyst.

The absorption peak at 664 nm decreased gradually with time as shown in Fig. 4a–c. Similar to the previous case, there is an initially slower degradation which accelerates with time, probably due to the removal of the CTAB from the Au NRs. Rate constants for sample.

R1, R2 and R3 were measured as 0.17692, 0.25597 and 0.44892 min^{-1}, respectively, by making a linear fit to the plot of Fig. 4d. Therefore, the degradation of dye is faster for Au NRs of higher aspect ratios. In this case, there is a 3.5 order increase in the rate of reaction when the aspect ratio of Au NRs was increased from 2.3 to 5.4.

Finally, we carried out the catalytic degradation of MO which is a common anionic azo dye [21, 30]. It is water-soluble and used to stain silk, wool, etc. Methyl orange is widely used in various fields from textiles to the pharmaceutical industry. But it is also a carcinogenic dye, therefore, its degradation into non-toxic dyes is crucial [31]. In an aqueous environment, MO shows maximum absorbance at 464 nm. This absorption peak at 464 nm decreases rapidly in the presence of $NaBH_4$ and Au NRs as shown in Fig. 5a–c which indicates its reductive degradation. A new peak at 248 nm appears which increases in intensity with time. This verifies the successful degradation of MO into two or more molecules with amine ($-NH_2$) [32]. Figure 5d depicts the variation of ln(C/C_0) with time. In this case, as well, there is a slight change in the slope with time, which could be due to the removal of the CTAB bilayer with the time that exposes

Fig. 3 Catalytic reduction of 4-NP using sample R1 (**a**), R2 (**b**) and R3 (**c**) as a catalyst; natural logarithm of relative intensity vs time plot (**d**)
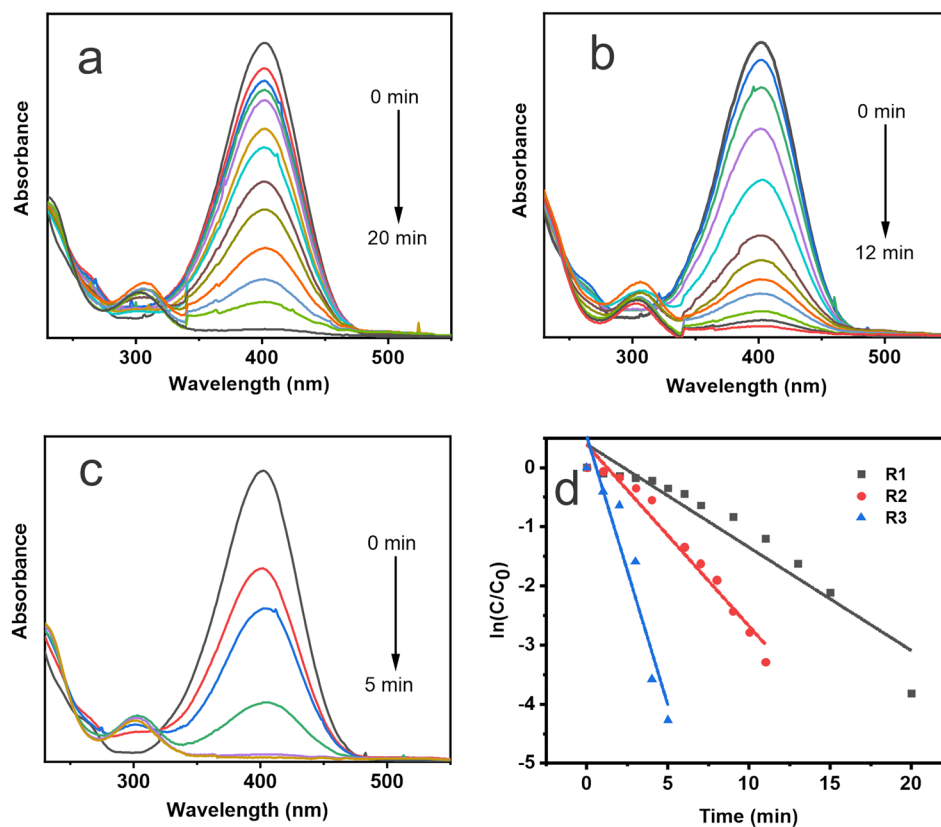

Fig. 4 Catalytic degradation of MB using samples R1 (**a**), R2 (**b**) and R3 (**c**) as a catalyst; natural logarithm of relative intensity vs time plot (**d**)
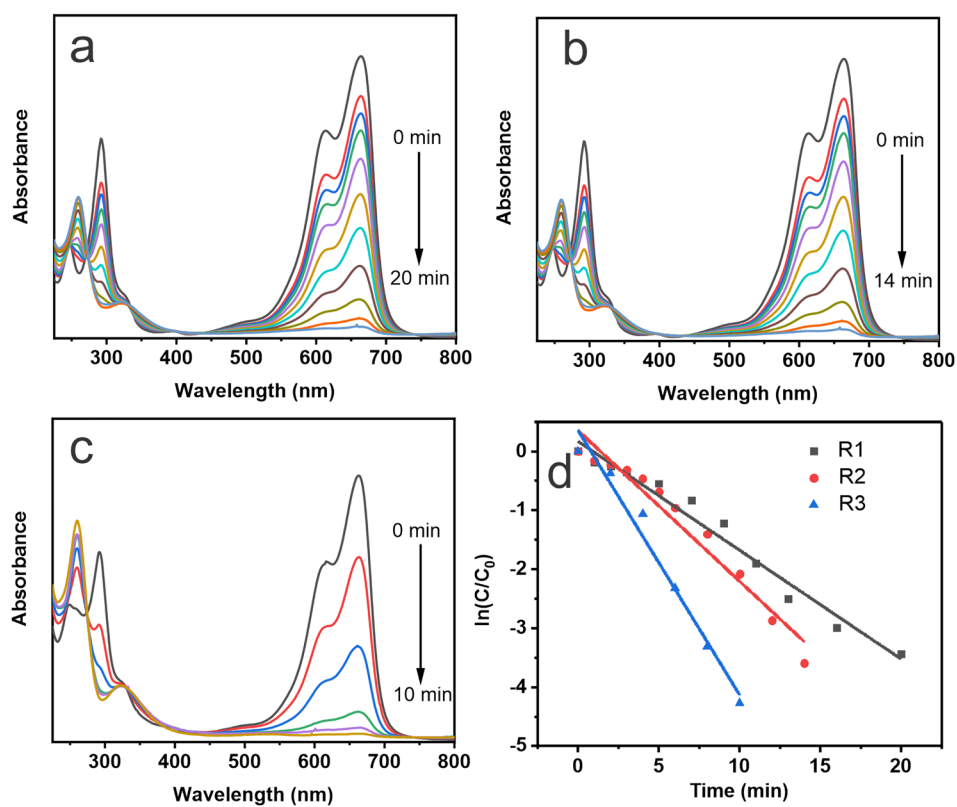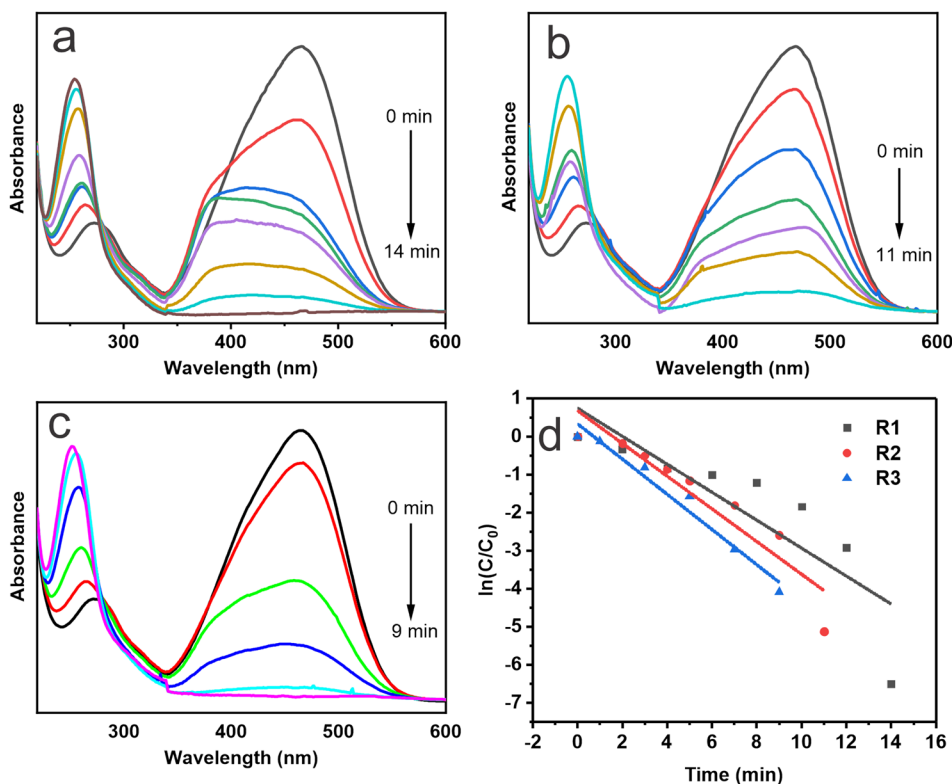
Fig. 5 Catalytic degradation of MO using samples R1 (**a**), R2 (**b**) and R3 (**c**) as a catalyst; natural logarithm of relative intensity vs time plot (**d**)

the active sites and accelerates catalysis, as discussed before. Rate constants for samples R1, R2 and R3 were 0.367, 0.429 and 0.462 min^{-1}, respectively. Although in this case there is not a marked difference in the degradation rates, they still increase with the increase in the aspect ratio of NRs.

3.2 Discussion

The surface energy of the gold nanoparticles depends sensitively on the type of facets. As mentioned before, the side facets of Au NRs have higher energy {520} compared to the end {111} and {100} facets which have relatively lower energy [14]. We have estimated the surface area of the side and end facets using a model depicted in Fig. 6. The AuNR can be approximated to consist of a cylinder with hemispherical endcaps. The surface area of the cylinder represents the surface area of the side facets, and the surface area of the hemispherical endcaps represents the surface area of the end facets. Below is the equation used to estimate the surface areas.

$$A = A_{cylinder} + A_{endcaps} \tag{1}$$

$$A = 2\pi(d/2)l + 4\pi(d/2)^2 \tag{2}$$

where $A_{cylinder}$ and $A_{endcaps}$ are the surface areas of the cylinder and endcaps, respectively. Moreover, l and d are the length of the cylindrical part and the diameter of the

Fig. 6 Nanorod's model used for the surface areas of calculation of side and end facets
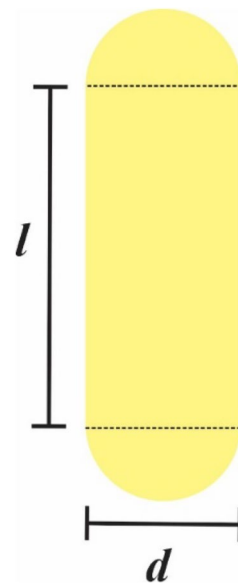
endcaps, respectively, which were calculated using TEM images. We have also estimated the total surface area of the NRs used for catalysis. Table 1 shows the respective values of the facets for the AuNRs samples. It is interesting to see that the overall surface area of the Au NRs decreased for R2, compared to R1, yet the catalytic activity of R2 is higher than R1 for all reactions. This can be rationalized by considering the relative surface area of the high-energy side facets for the two samples, which is much higher for R2 compared

Table 1 The surface area of Au NRs used for the catalytic reduction of 4-NP and MO. For MB, the values are twice as large as the ones given below

Sample	Surface area of a single NR(cm^2)	Number of NRs used in catalysis	Surface area of NRs used in catalysis (cm^2)	Surface area of side facets (cm^2)	Surface area of end facets (cm^2)
R1	1.91×10^{-11}	1.845×10^{11}	3.52	2.037	1.483
R2	3.2×10^{-11}	1.09×10^{11}	3.49	2.721	0.768
R3	2.9×10^{-11}	1.37×10^{11}	3.87	3.24	0.727

to R1. Therefore, it is concluded from this result that the availability of the high-energy surface can be a significant factor in the catalytic efficiency of the nanorods.

As discussed previously, many researchers have reported the use of NPS for catalytic reduction of various reactions with contradictory results. However, there are several assumptions in those comparative studies that may lead to these contradictions. For example, in some reports, it has been assumed that there is a complete conversion of Au ions into Au NPs and the molar concentration of the NP is assumed to be the same as that of the starting precursor molarity [11, 12]. This is usually not the case as the 100% conversion efficiency of Au ions to Au(0) is not achievable under most of the experimental conditions, and it even changes with a slight change in the reaction conditions e.g. with the variation in the pH of the growth solution, as seen in this study. Therefore, it is important to verify the Au content of each morphology before the comparative study. The current study also suggests that, in addition to the relative surface area, effect of the surface energy should be taken into account.

4 Conclusion

We have shown that the aspect ratio of Au NRs can be controlled with the variation of the pH of the growth solution. The slower growth kinetics favored the deposition of the Au atoms on the end facets of growing NRs and consequently resulted in the fabrication of higher aspect ratio Au NRs. The relative fraction of the high-energy side facets increases with the increase in the aspect ratio, which has a marked influence on the catalytic performance of Au NRs. The catalytic reduction of 4-NP, MB and MO by Au NRs depended sensitively on the aspect ratios of Au NRs. Nanorods with higher aspect ratios were more effective for catalysis in all cases due to the higher surface area of the high-energy side facets.

Declarations

Competing interests The authors declare no competing interests.

References

1. Yeh Y-C, Creran B, Rotello VM (2012) Gold nanoparticles: preparation, properties, and applications in bionanotechnology. Nanoscale 4(6):1871–1880
2. Wang X, Wu J-R, Liang F, Yang Y-W (2019) In situ gold nanoparticle synthesis mediated by a water-soluble leaning pillar [6] arene for self-assembly, detection, and catalysis. Org Lett 21(13):5215–5218
3. Alegria EC, Ribeiro AP, Mendes M, Ferraria AM, Do Rego AMB, Pombeiro AJ (2018) Effect of phenolic compounds on the synthesis of gold nanoparticles and its catalytic activity in the reduction of nitro compounds. Nanomaterials 8(5):320
4. Pérez-Juste J, Pastoriza-Santos I, Liz-Marzán LM, Mulvaney P (2005) Gold nanorods: synthesis, characterization and applications. Coord Chem Rev 249(17–18):1870–1901
5. Huang X, Neretina S, El-Sayed MA (2009) Gold nanorods: from synthesis and properties to biological and biomedical applications. Adv Mater 21(48):4880–4910
6. Bond GC, Sermon PA, Webb G, Buchanan DA, Wells PB (1973) Hydrogenation over supported gold catalysts. J Chem Soc, Chem Commun 13:444b-b445
7. Haruta M, Kobayashi T, Sano H, Yamada N (1987) Novel gold catalysts for the oxidation of carbon monoxide at a temperature far below 0 C. Chem Lett 16(2):405–408
8. Hutchings GJ (1985) Vapor phase hydrochlorination of acetylene: correlation of catalytic activity of supported metal chloride catalysts. J Catal 96(1):292–295
9. Priecel P, Salami HA, Padilla RH, Zhong Z, Lopez-Sanchez JA (2016) Anisotropic gold nanoparticles: preparation and applications in catalysis. Chinese J Catal 37(10):1619–50
10. Ishida T, Murayama T, Taketoshi A, Haruta M (2019) Importance of size and contact structure of gold nanoparticles for the genesis of unique catalytic processes. Chem Rev 120(2):464–525
11. Kundu S, Lau S, Liang H (2009) Shape-controlled catalysis by cetyltrimethylammonium bromide terminated gold nanospheres, nanorods, and nanoprisms. J Phys Chem C 113(13):5150–5156
12. Jiji S, Gopchandran K (2019) Shape dependent catalytic activity of unsupported gold nanostructures for the fast reduction of 4-nitroaniline. Colloid Interface Sci Commun 29:9–16
13. Zhang Q, Wang H (2014) Facet-dependent catalytic activities of Au nanoparticles enclosed by high-index facets. ACS Catal 4(11):4027–4033
14. Carbó-Argibay E, Rodríguez-González B, Gómez-Graña S, Guerrero-Martínez A, Pastoriza-Santos I, Pérez-Juste J et al (2010) The crystalline structure of gold nanorods revisited: evidence for higher-index lateral facets. Angew Chem 122(49):9587–9590

15. Kooij ES, Ahmed W, Zandvliet HJ, Poelsema B (2011) Localized plasmons in noble metal nanospheroids. J Phys Chem C 115(21):10321–10332

16. Scarabelli L, Sánchez-Iglesias A, Pérez-Juste J, Liz-Marzán LM (2015) A "tips and tricks" practical guide to the synthesis of gold nanorods. J Phys Chem Lett. https://doi.org/10.1021/acs.jpclett.5b02123

17. Busbee BD, Obare SO, Murphy CJ (2003) An improved synthesis of high-aspect-ratio gold nanorods. Adv Mater 15(5):414–416

18. Khan HI, Khan GA, Mehmood S, Khan AD, Ahmed W (2019) Gold nanoworms: optical properties and simultaneous sers and fluorescence enhancement. Spectrochim Acta Part A Mol Biomol Spectrosc 220:117111

19. Ahmed W, Öztürk İM, Iftikhar RMF, Bek A (2022) Seedless, size and shape controlled synthesis of gold mesoscopic particles and their excellent SERS applications. Mater Chem Phys 278:125589

20. Wei Q, Ji J, Shen J (2008) PH controlled synthesis of high aspect-ratio gold nanorods. J Nanosci Nanotechnol 8(11):5708–5714

21. Abdullah A, Altaf M, Khan HI, Khan GA, Khan W, Ali A et al (2018) Facile room temperature synthesis of multifunctional CTAB coated gold nanoparticles. Chem Phys 510:30–36

22. Wang S, Gao S, Tang Y, Wang L, Jia D, Liu L (2018) Facile solid-state synthesis of highly dispersed Cu nanospheres anchored on coal-based activated carbons as an efficient heterogeneous catalyst for the reduction of 4-nitrophenol. J Solid State Chem 260:117–123

23. Muench F, Rauber M, Stegmann C, Lauterbach S, Kunz U, Kleebe H-J et al (2011) Ligand-optimized electroless synthesis of silver nanotubes and their activity in the reduction of 4-nitrophenol. Nanotechnology 22(41):415602

24. Gazi S, Ananthakrishnan R (2011) Metal-free-photocatalytic reduction of 4-nitrophenol by resin-supported dye under the visible irradiation. Appl Catal B 105(3–4):317–325

25. He J, Unser S, Bruzas I, Cary R, Shi Z, Mehra R et al (2018) The facile removal of CTAB from the surface of gold nanorods. Colloids Surf, B 163:140–145

26. Mills A, Hazafy D, Parkinson J, Tuttle T, Hutchings MG (2011) Effect of alkali on methylene blue (CI Basic Blue 9) and other thiazine dyes. Dyes Pigm 88(2):149–155

27. Tahazadeh S, Karimi H, Mohammadi T, Emrooz HBM, Tofighy MA (2021) Fabrication of biodegradable cellulose acetate/MOF-derived porous carbon nanocomposite adsorbent for methylene blue removal from aqueous solutions. J Solid State Chem 299:122180

28. Noubactep C (2009) Characterizing the discoloration of methylene blue in Fe0/H$_2$O systems. J Hazard Mater 166(1):79–87

29. Khan GA, Esentürk EN, Bek A, Bhatti AS, Ahmed W (2021) Fabrication of highly catalytically active gold nanostructures on filter-paper and their applications towards degradation of environmental pollutants. ChemistrySelect 6(39):10655–10660

30. Fan J, Guo Y, Wang J, Fan M (2009) Rapid decolorization of azo dye methyl orange in aqueous solution by nanoscale zerovalent iron particles. J Hazard Mater 166(2–3):904–910

31. Ismail M, Gul S, Khan M, Khan MA, Asiri AM, Khan SB (2019) Green synthesis of zerovalent copper nanoparticles for efficient reduction of toxic azo dyes congo red and methyl orange. Green Process Synth 8(1):135–143

32. Sha Y, Mathew I, Cui Q, Clay M, Gao F, Zhang XJ et al (2016) Rapid degradation of azo dye methyl orange using hollow cobalt nanoparticles. Chemosphere 144:1530–1535

Authors and Affiliations

Lubna Khalil[1] · Sana Sabahat[1] · Waqqar Ahmed[2]

✉ Sana Sabahat
s.sabahat@comsats.edu.pk

✉ Waqqar Ahmed
w.ahmed@comsats.edu.pk

1 Department of Chemistry, COMSATS University Islamabad, Islamabad 45500, Pakistan

2 Materials Laboratory, Department of Physics, COMSATS University Islamabad, Islamabad 45500, Pakistan